Estimating the True Maximum Sustained Wind Speed of a Tropical Cyclone from Spatially Averaged Observations

DAVID MAYERS AND CHRISTOPHER RUF

University of Michigan, Ann Arbor, Michigan

(Manuscript received 16 July 2019, in final form 21 December 2019)

ABSTRACT

The maximum sustained wind speed Vm of a tropical cyclone (TC) observed by a sensor varies with its spatial resolution. If unaccounted for, the difference between the ''true'' and observed Vm results in an error in estimation of Vm. The magnitude of the error is found to depend on the radius of maximum wind speed Rm and Vm itself. Quantitative relationships are established between Vm estimation errors and the TC characteristics. A correction algorithm is constructed as a scale factor to estimate the true Vm from coarsely resolved wind speed measurements observed by satellites. Without the correction, estimates of Vm made directly from the observations have root-mean-square differences of 1.77, 3.41, and 6.11 m s^{-1} given observations with a spatial resolution of 25, 40, and 70 km, respectively. When the proposed scale factors are applied to the observations, the errors are reduced to 0.69, 1.23, and 2.12 m s^{-1}. A demonstration of the application of the correction algorithm throughout the life cycle of Hurricane Sergio in 2018 is also presented. It illustrates the value of having the scale factor depend on Rm and Vm, as opposed to using a fixed value, independent of TC characteristics.

1. Introduction

Spaceborne remote sensing is an excellent way to provide worldwide measurements of geophysical parameters, especially in remote locations. Satellite measurements are made at a variety of different spatial resolutions. When measurements of the same scene at different resolutions are used to estimate a characteristic, how are they to be compared? This paper examines this question for the case of measurements of ocean surface wind speed near a tropical cyclone (TC) that are used to estimate the 1-min maximum sustained wind speed Vm. The Vm, the basis for the Saffir–Simpson scale, is one of the primary metrics used to determine TC intensity. Scale factors are developed and used to estimate high-resolution Vm from low-resolution wind speed measurements. The scale factor is shown to be a function of storm intensity as well as the size of the pocket of highest wind speeds (the radius of maximum winds will be used as a proxy for this). We examine the dependence of the scale factor on these two TC properties and consider what information about a TC is lost by measuring at low resolution.

The idea of converting TC intensity parameters between spatial scales is similar to gust factors, which convert maximum sustained winds defined with respect to different temporal averaging intervals (e.g., between a 1- and 10-min-averaged gust). Gust factor is a well-established and well-researched topic (Harper et al. 2010), but little detailed research has been done for a similar idea concerning spatial averages. Gust factor is dependent on numerous other inputs, including the roughness length (exposure), distance from an upstream terrain change, stability, height above sea level, and, potentially, the presence of convection (Paulsen and Schroeder 2005). Similarly, this paper investigates the various dependencies of a spatial scale factor for Vm.

The ideas presented in this work are relevant to remote sensing measurements that attempt to use spatially coarse wind speed measurements to estimate a ''true'' (i.e., very high resolution) TC parameter. One class of such instruments is the scatterometer, which relates wind speed to the roughness of the ocean surface via Bragg resonance of the backscattered signal (Hilburn et al. 2006). Scatterometers typically operate

Denotes content that is immediately available upon publication as open access.

Corresponding author: David Mayers, drmayers@umich.edu

DOI: 10.1175/JAMC-D-19-0177.1

© 2020 American Meteorological Society. For information regarding reuse of this content and general copyright information, consult the AMS Copyright Policy (www.ametsoc.org/PUBSReuseLicenses).

at microwave frequencies with wavelengths of between 2 (Ku band) and 5 (C band) cm. It is worth noting that C band and Ku band are attenuated and scattered by raindrops (Ku band more than C band), and scatterometers also suffer from reduced performance in rain because of outflow from storms and the "splash effect" of raindrops roughening the ocean surface (Hilburn et al. 2006; Portabella et al. 2012; Stiles and Yueh 2002; Weissman and Bourassa 2008). Also, many scatterometers saturate at wind speeds above $\sim 30\,\mathrm{m\,s^{-1}}$ (Donelan et al. 2004; Hwang et al. 2013), although cross-polarization scatterometers have recently been shown to retain sensitivity to high wind speeds (Mouche et al. 2017). Examples (note that most acronyms in this paper that are not defined can be found online at https://www.ametsoc.org/PubsAcronymList) of scatterometers include ASCAT (C band, at ~25-km resolution; Figa-Saldaña et al. 2002), QuikSCAT (Ku band, at ~25-km resolution; Draper and Long 2002), Sentinel-1 synthetic aperture radar (SAR) (Attema et al. 2007), and RapidScat (Ku band, at ~20-km resolution; Durden and Perkovic-Martin 2017). Cyclone Global Navigation Satellite System (CYGNSS) also measures wind speeds by relating ocean roughness to surface wind. It does this at a spatial resolution similar to scatterometers by receiving GPS signals reflected from the ocean surface in a bistatic radar configuration (~25 km; L band; Ruf et al. 2016, 2019). These satellites and their respective frequencies and spatial resolutions are summarized in Table 1.

Another class of ocean wind speed instrument is the radiometer, which relates excess emissivity to the wind speed. Some of these instruments operate at a wavelength of 21 cm (L band), which enables penetration through rain. Examples include NASA's Soil Moisture Active Passive mission (SMAP; L band, at 40-km spatial resolution; Meissner et al. 2017; Entekhabi et al. 2010), ESA's Soil Moisture and Ocean Salinity mission (SMOS; L band, at ~43-km spatial resolution; Reul et al. 2012; Kerr et al. 2010), and NASA's Aquarius (L band, at ~100-km resolution; Lagerloef et al. 2008; Meissner et al. 2014). Radiometers operating at higher frequencies include JAXA's Advanced Microwave Scanning Radiometer (AMSR2; C band, at 35 km × 62 km resolution; Zabolotskikh et al. 2016), WindSat (6.8, 10.7, 18.7, 23.8, and 37.0 GHz, at ~30-km resolution; Gaiser et al. 2004), and the Stepped Microwave Frequency Radiometer (SFMR; C band, at ~3-km resolution; Uhlhorn and Black 2003). Note that all-weather wind retrievals are possible at C band by using multiple channels at C or X band to remove rain contamination that is present in each individual channel (Meissner and Wentz 2009; Zabolotskikh et al. 2015). SFMR, an airborne instrument typically flown on the NOAA "Hurricane Hunter" aircraft, uses six channels at C band to allow for wind speed measurements through intense rainfall (Uhlhorn and Black 2003).

TABLE 1. Examples of instruments that measure wind speeds at varying spatial resolutions.

Name	Class	Frequency	Spatial Resolution
ASCAT	Scatterometer	C band	25 km
QuikSCAT	Scatterometer	Ku band	25 km
RapidScat	Scatterometer	Ku band	20 km
CYGNSS	Bistatic radar	L band	25 km
SMAP	Radiometer	L band	40 km
SMOS	Radiometer	L band	45 km
Aquarius	Radiometer	L band	100 km
AMSR2	Radiometer	C band	50 km
WindSat	Radiometer	C/X band	35 km

Although spatial resolution conversion has not been studied in detail, it has been acknowledged. Meissner et al. (2017), Reul et al. (2016), and Zabolotskikh et al. (2016) encountered issues with spatial resolution while comparing radiometer winds (SMAP, SMOS, and AMSR-2, respectively) with best-track (Landsea and Franklin 2013) 1-min maximum sustained winds. National Hurricane Center (NHC) best tracks are poststorm analyses of the intensity, position, and size of TCs and represent an official historical record for each storm. The reanalysis utilizes all available data for the storm, including data with high latency that was not available in near–real time for the original operational forecast. Vm was systematically underestimated as compared with best track. To improve the comparison, each of these papers utilize a 0.93 scale factor from Harper et al. (2010). This is a gust factor that scales the 1-min sustained winds from best track to a 10-min sustained wind. Meissner argues this is acceptable because of the way radiometers are sensitive to wind speed—they relate wind speed to the excess emissivity, which is highly correlated with the roughness of the ocean. Meissner et al. (2017) argues that 10-min sustained winds are required for the ocean surface to fully respond to the wind speed. One study (Reul et al. 2016) even admits that, although the SMOS winds were calibrated using "H*Wind" 1-min sustained wind speeds, the 10-min sustained wind speeds compare better because of its coarse spatial resolution. They too applied the 0.93 gust factor. However, satellite measurements of wind speed are nearly instantaneous in time and averaged spatially, so perhaps temporal scaling by the gust factor may not be appropriate. Instead, a scale factor is considered to relate Vm at coarse resolution to the high-resolution Vm as reported by best track.

2. Dataset and processing methods

The Hurricane Weather Research and Forecasting (HWRF) system is an operational model implemented at the National Centers for Environmental Prediction of the National Weather Service to provide numerical guidance to the NHC for the forecasting of tropical cyclone track, intensity, and structure (Biswas et al. 2018). This study will utilize HWRF wind fields from all storms in all basins in 2017 and 2018. HWRF has a parent and two nested domains. This study will use the innermost nest with the finest resolution. The inner-nest domain covers about 5.9° × 5.9° centered on the storm with grid spacing of about 0.011° (about 1.5 km). This study only uses the HWRF initialization (rather than including all wind fields that were propagated forward in time by the HWRF model) so that the study is less dependent on the characteristics of the HWRF simulation. HWRF is initialized by assimilating conventional observations, tail Doppler Radar, satellite observations, and Global Data Assimilation System 6-hourly forecasts. The HWRF data used in this study are the 10-m wind speed along with the mean sea level pressure and the corresponding latitude and longitude of each grid point.

The TC parameters used in this study are the maximum wind speed (Vm) and the radius of maximum wind speed (Rm). Vm is simply the 1-min maximum sustained wind speed in the wind field (HWRF wind speeds are 1-min wind speeds). The Rm must be defined with respect to a storm center location. The storm center is established by identifying the point of minimum surface pressure; Rm is then calculated by averaging the distances to the 10 grid points of highest wind speed surrounding the storm center position after removing all outliers. This is more robust than simply using the radial distance of the grid point with maximum wind speed.

To explore how resolution affects these TC parameters, spatial averaging is performed. The native HWRF resolution of 1.5 km is assumed to be fine enough to provide true Vm and Rm values. The reduced-resolution cases that will be examined in this paper are 25, 40, 70, and 100 km. These values are representative of various spaceborne ocean wind sensors (Table 1). The spatial average at a point is a uniformly weighted average of all grid points within a circle centered at the point with a diameter equal to the resolution. An example of a spatially averaged wind field with 40-km resolution is shown in Fig. 1. Note how the fine features of the wind field are lost as a result of spatial averaging, and the peak wind speed is reduced.

Storms near land are not included in this study. HWRF tends to produce pockets of anomalously high wind speeds on the windward side of the land feature. This can cause large errors in wind radii and smaller, but significant, errors in Vm. For this reason, all cases with the inner nest within 20 km of land are not considered.

3. Scale-factor dependencies

We define the scale factor SF for maximum sustained wind speed Vm as the ratio between the value when derived from HWRF inner-nest wind speed data and the value when derived from spatially smoothed data at a coarser resolution. For example, the SF for spatially smoothed data with resolution R is given by

$$\mathrm{SF}_R = \mathrm{Vm}_0/\mathrm{Vm}_R, \tag{1}$$

where Vm_R is the maximum sustained wind speed value derived from the model data with spatial resolution of R, with Vm_0 indicating the native HWRF inner-nest data value. Note that an SF close to unity indicates that Vm is not significantly impacted by spatial smoothing. When an SF deviates significantly from unity, Vm is impacted and will be estimated incorrectly from smoothed data if no correction is made. This section examines which TC characteristics affect the SF and develops quantitative relationships to estimate Vm_0 from measurements made at coarser spatial resolution.

The relationship between the SF and the radius of maximum wind speed Rm is illustrated in Fig. 2. The figure shows a population of values for SF derived empirically from individual HWRF storms, together with a parametric curve fit by least squares through the points. Keep in mind that Rm is being used as a proxy for the size of the high-wind core. The SF is largest when Rm is small because a smaller pocket of high winds is affected more by spatial averaging. SF changes rapidly with Rm until Rm is much larger than the spatial resolution, after which the SF is fairly insensitive to changes in Rm. For these reasons, we assume the following functional relationship:

$$\mathrm{SF}_R(\mathrm{Rm}_R) = c + e^{-d\mathrm{Rm}_R}, \tag{2}$$

where c and d are tunable parameters. Least squares fits to the SF for 25-, 40-, 70-, and 100-km resolution were performed and the resulting curves are displayed in Fig. 3. SF can be seen to exhibit similar behavior at all spatial resolutions. In each case, the sensitivity of SF to Rm decreases significantly when Rm is larger than the spatial resolution. Note that the measured Rm below 30 and 40 km is not well defined with 70- and 100-km resolution, respectively, because, with such small storms,

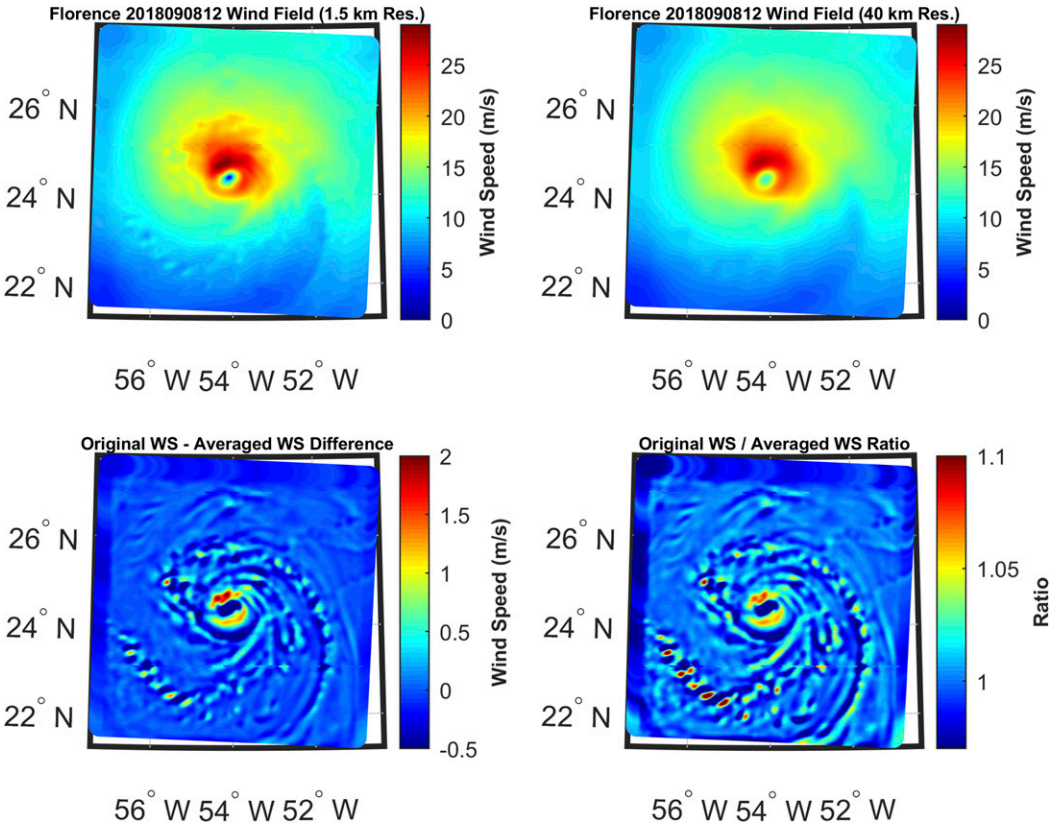


FIG. 1. The effects of spatial averaging on a TC wind field. (top left) Image of a high-resolution wind field using HWRF inner-nest native resolution (1.5-km resolution). (top right) Image that is spatially averaged over 40 km and is equivalent to what a wind-measuring satellite with 40-km resolution would observe. Note how the lower-resolution image loses the finer features that are present in the high-resolution image. (bottom left) The difference between the 40-km winds and the high-resolution winds. (bottom right) The ratio between the two wind fields in the top panels. The greatest differences occur around small-scale features such as the region of highest wind speeds, which is of particular interest for this paper.

very coarse resolution causes the maximum wind speed to lie at the storm center.

In Fig. 4, the relationship between SF and Vm is shown in a manner that is similar to that in Fig. 2. The SF can be seen to increase with Vm because Vm is correlated with storm size and organization. For example, when Vm is large, the TC tends to be intense and well-organized, with a small pocket of highest wind speeds. When Vm is small, storms tend to have a larger high wind speed area and are more loosely organized. Figure 4 demonstrates that SF depends strongly on Vm for weaker storms because this is where a relatively small change in Vm can drastically change the organization of the storm and, therefore, the size of the pocket of highest wind speeds. For large Vm, SF loses sensitivity to Vm. The behavior of the dependence suggests a parametric model of the form

$$\mathrm{SF}_R(\mathrm{Vm}_R) = a - e^{-b\mathrm{Vm}_R}. \tag{3}$$

Figure 5 shows the resulting parametric model when fit to SF as a function of Vm with a spatial resolution of 25, 40, 70, and 100 km. The same general behavior is again found, with SF increasing as spatial resolution coarsens.

The dependence of SF on Vm and Rm can be combined into a more general parametric model of the form

$$\mathrm{SF}_R(\mathrm{Rm}_R, \mathrm{Vm}_R) = a(\mathrm{Rm}_R) - e^{-b(\mathrm{Rm}_R)\mathrm{Vm}_R}. \tag{4}$$

The dependence of a and b on Rm is determined by separating the dataset into Rm bins and fitting Eq. (3) to each group of data. A model of the form

$$a(\mathrm{Rm}) = k(\mathrm{Rm}^l) + m \tag{5}$$

is fit to each parameter (both a and b), with k, l, and m as constant real numbers. The resulting dependence of a and b on Rm is shown in Fig. 6. Parameter a is the asymptotic value of the function and effectively shifts the

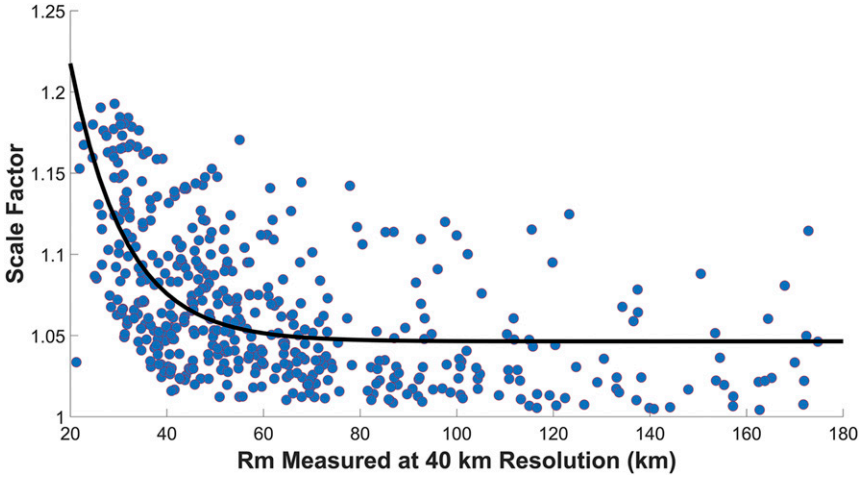


FIG. 2. There is a strong dependence of SF on radius of maximum wind speed. When Rm is at or below the spatial resolution, the SF exponentially decays with Rm. Once Rm is significantly greater than the SF, the SF loses sensitivity to Rm.

SF up and down; it decreases with Rm because, at larger Rm, the storm is less affected by averaging and therefore the SF is close to 1. Parameter b controls how quickly the SF achieves its asymptotic value; it increases with Rm, suggesting that the asymptotic value of SF is reached more quickly for storms with large areas of high wind speed. This is because Vm has little effect on SF when Rm is much larger than the spatial resolution. These power series relations are used to generate a 3D SF, which is shown in Fig. 7 as a contour plot. The 3D SF is maximized when Rm is small and Vm is large, and SF is minimized when Rm is large and Vm is small.

The parametric relationships can be used in a correction algorithm to estimate Vm_0 from coarse measurements of the wind field. In practice, when a satellite measures the wind field of a TC at spatial resolution R, estimates of the parameters Vm_R and Rm_R can be produced directly from the measurements. Using Rm_R and/or Vm_R as inputs to the correction algorithm, the appropriate value for SF is determined. This SF corrects,

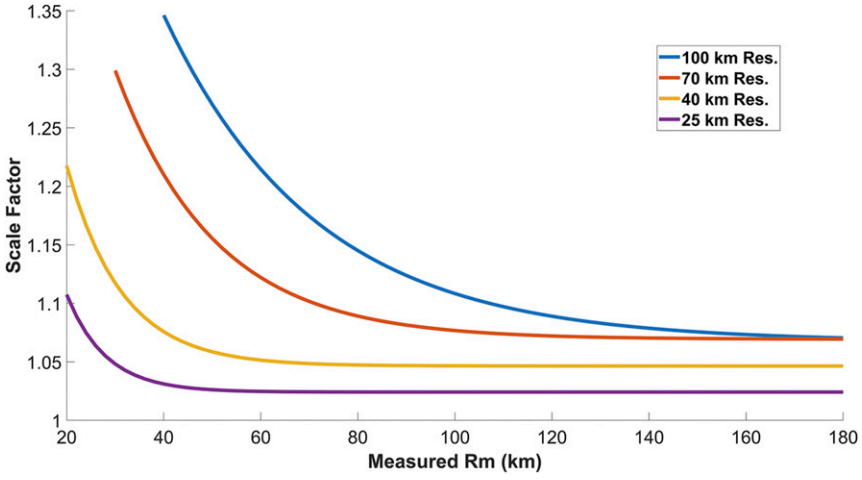


FIG. 3. The SF varies with Rm for different spatial resolutions. For each spatial resolution, SF(Rm) follows the same general trend. When Rm is at or below the spatial resolution, SF exponentially decays with Rm. Once Rm is significantly greater than SF, SF loses sensitivity to Rm, which leads to an asymptote. Note that a coarser spatial resolution corresponds to a higher SF. Also note that SF(Rm) is not defined for Rm $<$ 30 km at 70-km resolution and for Rm $<$ 40 km at 100-km resolution. This is because, at coarse resolution, smaller storms become so washed out that Rm cannot be determined.

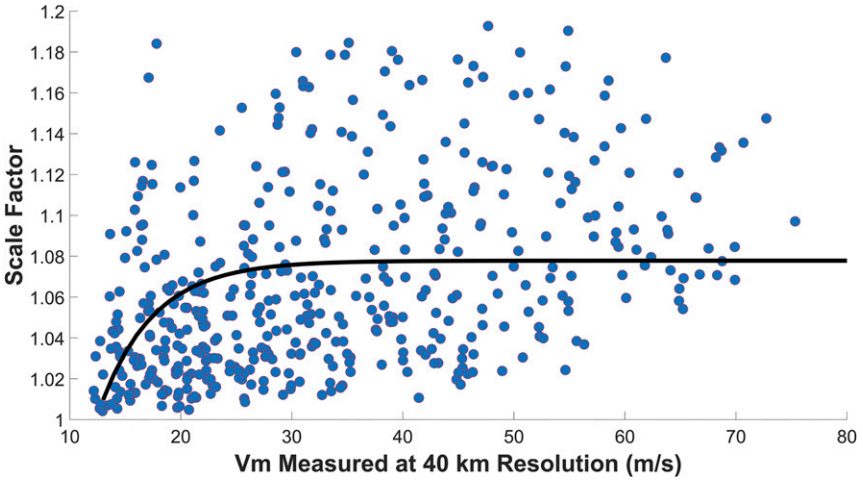


FIG. 4. There is a weak dependence of the SF on the maximum sustained wind speed, but the general trend is noteworthy. When Vm is large, the storm is typically small and well-organized and is greatly affected by spatial averaging. When Vm is small, the storm is typically loosely organized and large and is not affected much by spatial averaging.

or scales, the measured Vm_R to provide a better estimate of the true Vm_0. This procedure has been performed for all storms in the Atlantic, east Pacific, and west Pacific basins from 2017 and 2018. Half of the cases are randomly chosen as the training set for the parametric model. The other half are used to evaluate the performance of the correction. The root-mean-squared difference (RMSD) between the true Vm_0 and the Vm_0 estimated from spatially smoothed measurements are summarized in Table 2. The first row of the table states the RMSD if no correction is made (i.e., using an SF of unity). As noted above, errors are larger with coarser spatial resolution. The second row is the RMSD for the simplest correction method—applying a constant SF, as in Eq. (1), which is derived for a particular spatial resolution but does not depend on Rm, Vm, or any other parameter. Use of a constant SF does reduce the RMSD significantly, so it is much better than no correction. The remaining lines of Table 2 report RMSD values produced when more sophisticated versions of the SF correction are used that depend on properties of the storm that are directly measurable at the coarser resolution. Of the correction algorithms that depend on only one storm property, the one dependent on Rm performs

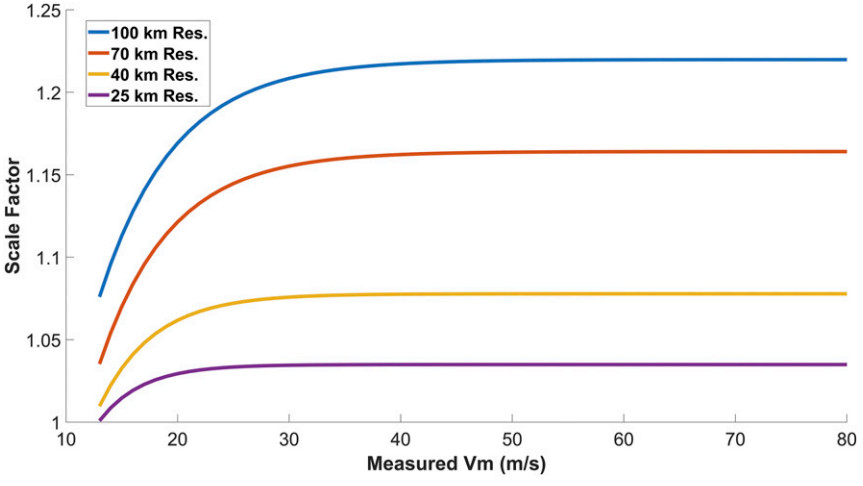


FIG. 5. The SF varies with Vm at different spatial resolutions: SF increases as spatial resolution coarsens, it is large for high-intensity cases in which the storm is typically small and well-organized, and it is small for low-intensity cases in which the storm is typically large and disorganized with a large pocket of highest wind speeds.

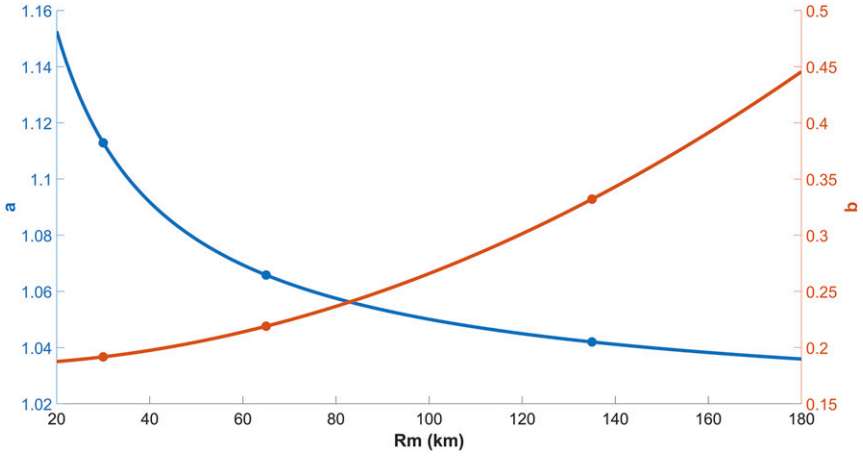


FIG. 6. The dependence of the parameters a and b on Rm is used to extend the SF to three dimensions. Parameter a is the asymptotic value of SF and effectively shifts SF up and down; it decreases with Rm because, at larger Rm, the storm is less affected by averaging and therefore SF is small. Parameter b controls how quickly SF achieves its asymptotic value; it increases with Rm, suggesting that the asymptotic value of SF is reached more quickly for large storms. This is because Vm has little effect on SF when Rm is much larger than the spatial resolution.

best. This suggests that storm size is more highly correlated with changes in SF than is storm intensity. A better correction yet uses both Rm and Vm to estimate SF. For this correction method, the resulting RMSD values are listed in the last row of Table 2. It effectively combines both dependencies shown in Figs. 2 and 4. The RMSD values are 0.69, 1.23, and 2.12 m s^{-1} for 25, 40, and 70 km, respectively. Note that results requiring Rm as input are not listed for 100-km spatial resolution because many of the individual cases have Rm values of zero as a result of significant averaging of the wind field. In such cases (e.g., in the case of Aquarius measurements of the wind field) (Meissner et al. 2014), some other SF dependence should be considered, such as only Vm.

The effect of the correction SF(Rm, Vm) is visualized in Fig. 8. The red dots are the best-track Vm values matched up with Vm measured by a 40-km-resolution instrument (note this figure only includes the test cases—not the cases that were used to train the SF surface). These matchups typically remain under the 1-to-1 line because Vm is underestimated without an SF correction. The blue dots, the matchups after SF correction, are much closer to the 1-to-1 line. This figure shows the necessity of SF correction when estimating Vm from

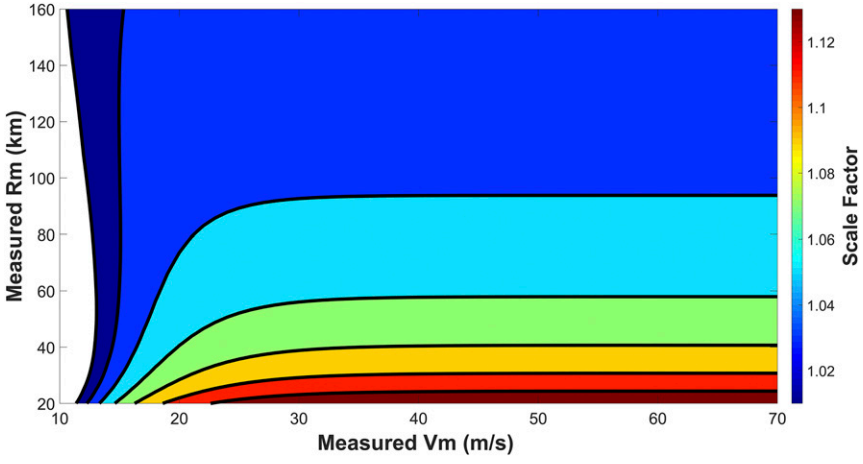


FIG. 7. A slice of the three-dimensional SF at 40-km resolution, illustrating its dependence on Vm and Rm. The SF reaches a maximum value of 1.15 when Rm is small and Vm is large. The 3D SF combines trends seen previously in Figs. 2 and 4. The solid black lines indicate contours of constant SF.

TABLE 2. The root-mean-square difference in wind speed ($m\,s^{-1}$) between true and measured Vm with varying types of correction applied to the measured Vm, for different spatial resolution of the measurements. Cases considered are no correction, a constant SF for a particular spatial resolution, and SF corrections that depend on Vm, Rm, and both Vm and Rm. The "LMS Rm, Vm" row shows the results with Vm dependence for three different sizes of Rm: large, medium, and small.

		Resolution			
Dependence	Equation no.	25 km	40 km	70 km	100 km
No Correction	—	1.77	3.41	6.12	6.61
Constant	—	0.87	1.61	2.80	2.90
Vm	(3)	0.83	1.57	2.66	2.72
LMS Rm, Vm	—	0.74	1.33	2.26	—
Rm	(2)	0.75	1.28	2.16	—
Rm, Vm	(4)	0.69	1.23	2.12	—

coarse-resolution measurements. Figure 8 also demonstrates increased scatter at high winds. The RMS error between the best-track Vm and the Vm estimated from 40-km wind speed measurements is 0.65, 1.42, and 1.91 $m\,s^{-1}$ for best-track Vm below 30 $m\,s^{-1}$, between 30 and 45 $m\,s^{-1}$, and greater than 45 $m\,s^{-1}$, respectively. The error increases as storm intensity increases as seen in Fig. 8. Similarly, the RMS error at 40-km resolution is 1.63, 1.12, and 0.69 $m\,s^{-1}$ for best-track Rm less than 50 km, between 50 and 85 km, and greater than 85 km, respectively.

The radius of maximum wind speed, Rm, is shown to be strongly correlated with the SF correction. However, it is worth mentioning the deficiencies of using Rm as input in the correction algorithm. First, Rm is not included in the set of TC parameters that are best tracked (because Rm is primarily used to initialize models). Second, it is difficult to estimate Rm from an observed wind field that is fraught with noise and sampling gaps. This task becomes even more difficult when considering that a reliable estimate of Rm requires both an accurate storm center location and an accurate maximum wind speed location. The uncertainties of best-track storm center locations are about 65, 40, and 27 km for tropical storms, category-2 storms, and category-4/5 storms, respectively (Torn and Snyder 2012). The combination of this storm center uncertainty with the uncertainty in maximum wind speed location makes estimating Rm difficult.

Despite these drawbacks, it is clear that the SF correction has improved performance when using Rm as input because Rm contains so much information about the size of the high–wind speed core. When a precise estimate of Rm is not available, it is still best to use as much information as possible about the size of the pocket of highest wind speeds in the SF correction algorithm. To demonstrate this, divide the population of storms into three groups of Rm: large, medium, and small. Define large Rm as Rm $>$ 80 km, small Rm as Rm $<$ 45 km, and medium Rm as everything between. Each of these three groups has a different SF curve that depends on Vm. The training set determines these curves, then the resulting SF is evaluated on the test set. The resulting test set errors, shown in Table 2, are comparable in performance with the SF correction

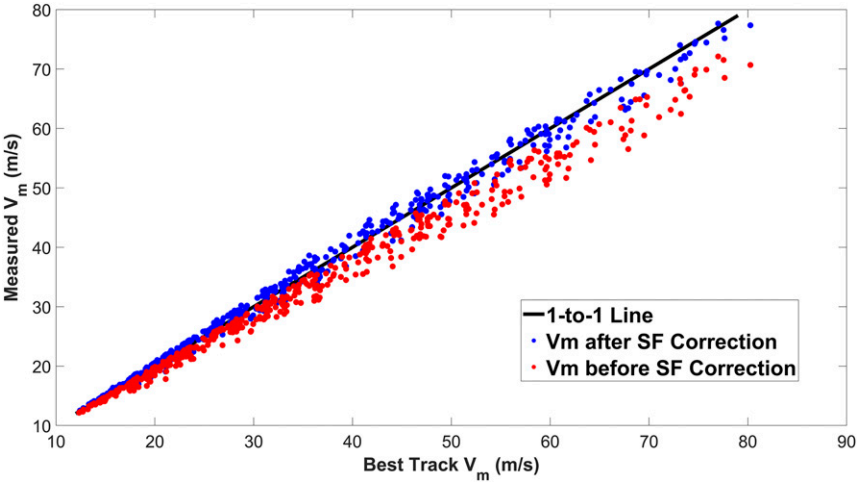


FIG. 8. Comparison of best-track Vm with the Vm measured at 40-km spatial resolution. The red dots (before SF correction) consistently underestimate Vm. The blue dots (after SF correction) are shifted up toward the 1-to-1 line (a perfect estimate). Note the increased scatter at higher Vm. Also note that only the test cases are plotted here. None of the training cases were included in this figure.

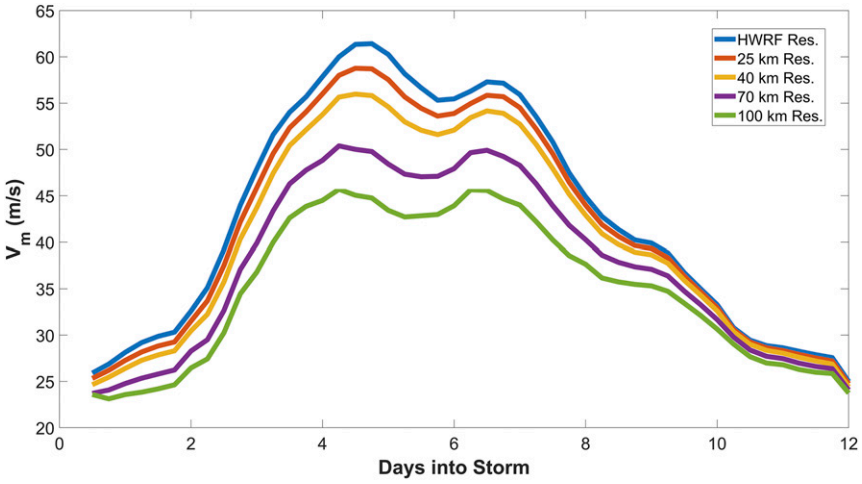


FIG. 9. Maximum sustained wind speed observed at different spatial resolutions throughout the lifetime of Hurricane Sergio, a major hurricane in the eastern Pacific basin (2018). The wide range of observed Vm values allows for analysis of the performance of the SF correction in different situations. Note that Vm strictly decreases as the spatial resolution coarsens.

methods that depend on a precise value of Rm, and perform much better than the SF correction that depends only on Vm. Yes, performance degrades when Rm is not known. But even coarse knowledge of the size of the high–wind speed core greatly improves SF performance and, therefore, estimation of a storm's maximum wind speed.

4. Example

Use of the scale factor is demonstrated with eastern Pacific Ocean Hurricane Sergio throughout its life cycle in 2018. The storm was chosen because it remained over open ocean for the bulk of its lifetime, which allows for a continuous analysis (recall the land flag). Hurricane Sergio also went through a wide range of sizes and intensities, which provides the opportunity to examine SF performance in many different circumstances.

Figure 9 contains Vm estimates over the lifetime of the storm derived from HWRF winds averaged to various spatial resolutions. Note that Vm always decreases as spatial resolution becomes coarser. Also note that the ratio between the blue line (Vm at HWRF inner-nest native resolution) and the other lines (Vm at coarser resolutions) represents the exact SFs that would be needed for perfect correction of Vm to account for averaging of the TC wind field. Estimates of these SFs are generated using the parametric model described above. Results are shown in Fig. 10 for 70-km resolution. The solid lines represent Vm at 1.5- and 70-km resolution. There is a wide gap between the two lines. Three different SFs are applied to the 70-km estimate: 1) SF(Vm) is the purple dotted line, 2) SF(Rm) is the yellow dotted line, and 3) SF(Rm, Vm) is the green dashed line. Note that SF(Rm, Vm) provides the best correction (error of 1.43 $m\,s^{-1}$). SF(Rm) (error of 4.23 $m\,s^{-1}$) performs worse than SF(Vm) (error of 2.11 $m\,s^{-1}$), although the cumulative error analysis in the previous section showed that SF(Rm) typically outperforms SF(Vm). This discrepancy is due to the fact that Hurricane Sergio is more intense than the average TC. SF(Rm) is averaged across all Vm, so it performs the best when Vm is near its average value. Because Hurricane Sergio is a more intense storm, SF(Rm) tends to underestimate Vm. In the later part of the storm, however, SF(Rm) performs well while SF(Vm) overestimates Vm. This is in part due to Vm becoming closer to average as the storm weakens. The radius of maximum winds estimated at different spatial resolutions is shown in Fig. 11 over the lifetime of Hurricane Sergio. In the later part of the storm, Rm is very large (near 100 km). When Rm is this large, the SF should be close to unity, but SF(Vm) does not account for storm size and overestimates Vm. Both SF(Rm) and SF(Vm, Rm) are able to give a better estimate of Vm during this stage of the storm than SF(Vm). Because SF(Vm, Rm) combines the strengths of SF(Rm) and SF(Vm), it performs well in all circumstances experienced with Hurricane Sergio.

5. Discussion and conclusions

This work examines the effects of spatial averaging on a TC wind field and, consequently, on the maximum sustained wind speed estimated from the smoothed observations. Estimation of the true Vm from coarse wind measurements is improved by multiplication of the

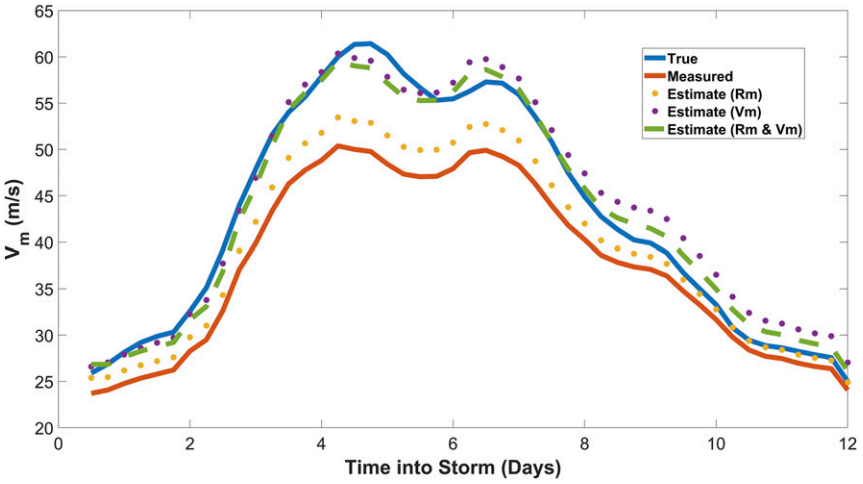


FIG. 10. The solid blue line is the true Vm over the lifetime of Hurricane Sergio. The solid orange line is Vm after averaging the wind field down from 1.5-km resolution to 70-km resolution. The other three lines are different estimates of Vm. The purple dotted line estimates Vm by applying an SF that is a function only of Vm. The yellow dotted line estimates Vm using an SF that is a function only of Rm. The dashed green line estimates Vm using an SF that is a function only of both Rm and Vm. This last estimation technique performs best.

observed Vm by a scale factor that is greater than unity. The optimal SF is found to depend on TC parameters Vm and Rm, with the strongest dependence on Rm. Rm works well as input to the SF correction because it operates as a proxy for the size of the high–wind speed core.

The mean SF (with dependence on both Vm and Rm) across all test cases is 1.03, 1.07, 1.14, and 1.18 for spatial resolutions of 25, 40, 70, and 100 km, respectively. The gust-factor conversion between a 1-min averaged gust and a 10-min averaged gust is 1.07 [Harper et al. 2010, p. 5 (their Table 1.2)]. This suggests that, on average, spatial smoothing over a 40-km area is roughly consistent with temporal averaging over 10 min in terms of their impact on Vm.

Note that the TC parameters used as input are those observed with coarse spatial resolution, so the implementation of this SF-based correction would be straightforward. When Rm is less than or equal to the spatial resolution of the measurements, SF decreases as Rm increases. When Rm is much greater than the spatial resolution, SF loses its dependence on Rm because the high wind speed region becomes large enough that the spatial averaging has negligible impact on Vm. SF, while not as dependent on Vm as Rm, increases as Vm

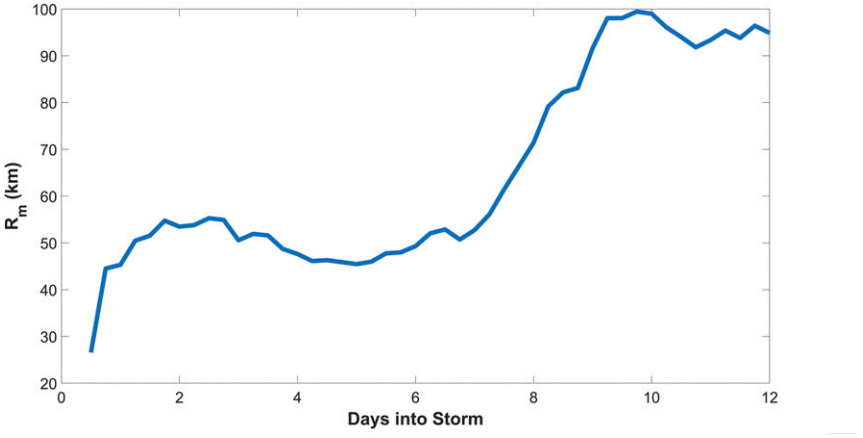


FIG. 11. The radius of maximum wind speed for Hurricane Sergio derived from the wind field at HWRF native resolution. The Rm becomes very large toward the end of the storm, which causes large errors in the estimation of Vm when the SF is not a function of Rm.

increases. This is because intense storms tend to be small and are more affected by spatial averaging.

Application of the SF correction throughout the life cycle of Hurricane Sergio is used to illustrate how inclusion of the dependencies on Rm and Vm improves the accuracy of the correction. When Hurricane Sergio is a major hurricane, inclusion of a Vm-dependent SF prevents significant underestimation of the true Vm. When the high wind speed region of Hurricane Sergio becomes very large (Rm $\sim$ 100 km), inclusion of an Rm-dependent SF prevents a significant overestimation of the true Vm.

An additional strategy is implemented to demonstrate that precise knowledge of Rm is not necessary for the SF correction to improve Vm estimated from coarse satellite measurements. Storms are classified as having a large, medium, or small high–wind speed core, and each of these three classes has a different SF correction that is dependent on Vm. Even with using these rough estimates of Rm, there is significant improvement over both a constant SF and SF(Vm). The best SF correction uses as much information as possible about the size of Rm, or the high-wind core, but even a rough estimate of Rm can greatly improve results.

Acknowledgments. The work presented was supported in part by NASA Science Mission Directorate Contract NNL13AQ00C with the University of Michigan.

REFERENCES

Attema, E., and Coauthors, 2007: Sentinel-1—The radar mission for GMES operational land and sea services. *ESA Bull.*, **131**, 10–17, https://ui.adsabs.harvard.edu/abs/2007ESABu.131...10A.

Biswas, M. K., L. Carson, K. Newman, D. Stark, E. Kalina, E. Grell, and J. Frimel, 2018: Community HWRF users' guide V4.0a. Developmental Testbed Center Rep., 162 pp., https://dtcenter.org/HurrWRF/users/docs/users_guide/HWRF-UG-2018.pdf.

Donelan, M. A., B. K. Haus, N. Reul, W. J. Plant, M. Stiassnie, H. C. Graber, O. B. Brown, and E. S. Saltzman, 2004: On the limiting aerodynamic roughness of the ocean in very strong winds. *Geophys. Res. Lett.*, **31**, L18306, https://doi.org/10.1029/2004GL019460.

Draper, D. W., and D. G. Long, 2002: An assessment of SeaWinds on QuikSCAT wind retrieval. *J. Geophys. Res.*, **107**, 3212, https://doi.org/10.1029/2002JC001330.

Durden, S. L., and D. Perkovic-Martin, 2017: The RapidScat ocean winds scatterometer: A radar system engineering perspective. *IEEE Geosci. Remote Sens. Mag.*, **5**, 36–43, https://doi.org/10.1109/MGRS.2017.2678999.

Entekhabi, D., and Coauthors, 2010: The Soil Moisture Active Passive (SMAP) mission. *Proc. IEEE*, **98**, 704–716, https://doi.org/10.1109/JPROC.2010.2043918.

Figa-Saldaña, J., J. J.W. Wilson, E. Attema, R. Gelsthorpe, M. R. Drinkwater, and A. Stoffelen, 2002: The advanced scatterometer (ASCAT) on the meteorological operational (MetOp) platform: A follow on for European wind scatterometers. *Can. J. Remote Sens.*, **28**, 404–412, https://doi.org/10.5589/m02-035.

Gaiser, P. W., and Coauthors, 2004: The WindSat spaceborne polarimetric microwave radiometer: Sensor description and early orbit performance. *IEEE Trans. Geosci. Remote Sens.*, **42**, 2347–2361, https://doi.org/10.1109/TGRS.2004.836867.

Harper, B. A., J. D. Kepert, and J. D. Ginger, 2010: Guidelines for converting between various wind averaging periods in tropical cyclone conditions. World Metrological Organization Tech. Doc. WMO/TD-1555, 64 pp., https://www.wmo.int/pages/prog/www/tcp/documents/WMO_TD_1555_en.pdf.

Hilburn, K., F. Wentz, D. Smith, and P. Ashcroft, 2006: Correcting active scatterometer data for the effects of rain using passive radiometer data. *J. Appl. Meteor. Climatol.*, **45**, 382–398, https://doi.org/10.1175/JAM2357.1.

Hwang, P., D. Burrage, D. Wang, and J. Wesson, 2013: Ocean surface roughness spectrum in high wind condition for microwave backscatter and emission computations. *J. Atmos. Oceanic Technol.*, **30**, 2168–2188, https://doi.org/10.1175/JTECH-D-12-00239.1.

Kerr, Y. H., and Coauthors, 2010: The SMOS mission: New tool for monitoring key elements of the global water cycle. *Proc. IEEE*, **98**, 666–687, https://doi.org/10.1109/JPROC.2010.2043032.

Lagerloef, G., and Coauthors, 2008: The Aquarius/SAC-D mission: Designed to meet the salinity remote-sensing challenge. *Oceanography*, **21**, 68–81, https://doi.org/10.5670/oceanog.2008.68.

Landsea, C. W., and J. L. Franklin, 2013: Atlantic hurricane database uncertainty and presentation of a new database format. *Mon. Wea. Rev.*, **141**, 3576–3592, https://doi.org/10.1175/MWR-D-12-00254.1.

Meissner, T., and F. J. Wentz, 2009: Wind-vector retrievals under rain with passive satellite microwave radiometers. *IEEE Trans. Geosci. Remote Sens.*, **47**, 3065–3083, https://doi.org/10.1109/TGRS.2009.2027012.

——, ——, and L. Ricciardulli, 2014: The emission and scattering of L-band microwave radiation from rough ocean surfaces and wind speed measurements from the Aquarius sensor. *J. Geophys. Res. Oceans*, **119**, 6499–6522, https://doi.org/10.1002/2014JC009837.

——, L. Ricciardulli, and F. J. Wentz, 2017: Capability of the SMAP mission to measure ocean surface winds in storms. *Bull. Amer. Meteor. Soc.*, **98**, 1660–1677, https://doi.org/10.1175/BAMS-D-16-0052.1.

Mouche, A. A., B. Chapron, B. Zhang, and R. Husson, 2017: Combined co- and cross-polarized SAR measurements under extreme wind conditions. *IEEE Trans. Geosci. Remote Sens.*, **55**, 6746–6755, https://doi.org/10.1109/TGRS.2017.2732508.

Paulsen, B. M., and J. L. Schroeder, 2005: An examination of tropical and extratropical gust factors and the associated wind speed histograms. *J. Appl. Meteor.*, **44**, 270–280, https://doi.org/10.1175/JAM2199.1.

Portabella, M., A. Stoffelen, W. Lin, A. Turiel, A. Verhoef, J. Verspeek, and J. Ballabrera-Poy, 2012: Rain effects on ASCAT-retrieved winds: Toward an improved quality control. *IEEE Trans. Geosci. Remote Sens.*, **50**, 2495–2506, https://doi.org/10.1109/TGRS.2012.2185933.

Reul, N., J. Tenerelli, B. Chapron, D. Vandemark, Y. Quilfen, and Y. Kerr, 2012: SMOS satellite L-band radiometer: A new capability for ocean surface remote sensing in

hurricanes. *J. Geophys. Res.*, **117**, C02006, https://doi.org/10.1029/2011JC007474.

——, B. Chapron, E. Zabolotskikh, C. Donlon, Y. Quilfen, S. Guimbard, J. F. Piolle, 2016: A revised L-band radio-brightness sensitivity to extreme winds under tropical cyclones: The five year SMOS-storm database. *Remote Sens. Environ.*, **180**, 274–291, https://doi.org/10.1016/j.rse.2016.03.011.

Ruf, C. S., and Coauthors, 2016: New ocean winds satellite mission to probe hurricanes and tropical convection. *Bull. Amer. Meteor. Soc.*, **97**, 385–395, https://doi.org/10.1175/BAMS-D-14-00218.1.

——, S. Asharaf, R. Balasubramaniam, S. Gleason, T. Lang, D. McKague, D. Twigg, and D. Waliser, 2019: In-orbit performance of the constellation of CYGNSS hurricane satellites. *Bull. Amer. Meteor. Soc.*, **100**, 2009–2023, https://doi.org/10.1175/BAMS-D-18-0337.1.

Stiles, B. W., and S. H. Yueh, 2002: Impact of rain on spaceborne Ku-band wind scatterometer data. *IEEE Trans. Geosci. Remote Sens.*, **40**, 1973–1983, https://doi.org/10.1109/TGRS.2002.803846.

Torn, R. D., and C. Snyder, 2012: Uncertainty of tropical cyclone best-track information. *Wea. Forecasting*, **27**, 715–729, https://doi.org/10.1175/WAF-D-11-00085.1.

Uhlhorn, E. W., and P. G. Black, 2003: Verification of remotely sensed sea surface winds in hurricanes. *J. Atmos. Oceanic Technol.*, **20**, 99–116, https://doi.org/10.1175/1520-0426(2003)020<0099:VORSSS>2.0.CO;2.

Weissman, D. E., and M. A. Bourassa, 2008: Measurements of the effect of rain-induced sea surface roughness on the QuikSCAT scatterometer radar cross section. *IEEE Trans. Geosci. Remote Sens.*, **46**, 2882–2894, https://doi.org/10.1109/TGRS.2008.2001032.

Zabolotskikh, E. V., L. M. Mitnik, N. Reul, and B. Chapron, 2015: New possibilities for geophysical parameter retrievals opened by GCOM-W1 AMSR2. *IEEE J. Sel. Top. Appl. Earth Obs. Remote Sens.*, **8**, 4248–4261, https://doi.org/10.1109/JSTARS.2015.2416514.

——, N. Reul, and B. Chapron, 2016: Geophysical model function for the AMSR2 C-band wind excess emissivity at high winds. *IEEE Geosci. Remote Sens. Lett.*, **13**, 78–81, https://doi.org/10.1109/LGRS.2015.2497463.